

Experimental and theoretical investigation of the crossover from the ultracold to the quasiclassical regime of photodissociation

I. Majewska,¹ S. S. Kondov,² C.-H. Lee,² M. McDonald,^{2,*} B. H. McGuyer,^{2,†} R. Moszynski,¹ and T. Zelevinsky^{2,‡}

¹*Quantum Chemistry Laboratory, Department of Chemistry, University of Warsaw, Pasteura 1, 02-093 Warsaw, Poland*

²*Department of Physics, Columbia University, 538 West 120th Street, New York, New York 10027-5255, USA*



(Received 22 May 2018; published 2 October 2018)

At ultralow energies, atoms and molecules undergo collisions and reactions that are best described in terms of quantum-mechanical wave functions. In contrast, at higher energies these processes can be understood quasiclassically. Here, we investigate the crossover from the quantum-mechanical to the quasiclassical regime both experimentally and theoretically for photodissociation of ultracold diatomic strontium molecules. This basic reaction is carried out with a full control of quantum states for the molecules and their photofragments. The photofragment angular distributions are imaged and calculated by using a quantum-mechanical model as well as the Wenzel–Kramers–Brillouin approximation and a semiclassical approximation that are explicitly compared across a range of photofragment energies. The reaction process is shown to converge to its high-energy (axial-recoil) limit when the energy exceeds the height of any reaction barriers. This phenomenon is quantitatively investigated for two-channel photodissociation by using intuitive parameters for the channel amplitude and phase. While the axial-recoil limit is generally found to be well described by a commonly used quasiclassical model, we find that when the photofragments are identical particles, their bosonic or fermionic quantum statistics can cause this model to fail, requiring a quantum-mechanical treatment even at high energies.

DOI: [10.1103/PhysRevA.98.043404](https://doi.org/10.1103/PhysRevA.98.043404)

I. INTRODUCTION

Low-temperature atomic and molecular collisions and reactions are qualitatively different from their high-energy counterparts. While the latter can usually be explained quasiclassically, the former are strongly influenced by the wave nature of the particles and are correctly described only with quantum-mechanical wave functions. In addition, at very low temperatures, precise control of internal molecular states is possible, permitting studies of state-specific reaction cross sections rather than statistical averages. Ultracold, quantum-mechanical chemistry has many distinguishing features such as reaction-barrier tunneling, quantum interference, and possibilities for controlling the outcome with applied electric or magnetic fields [1]. On the other hand, a quasiclassical interpretation can offer intuitive insight into complicated processes.

In particular, photodissociation [2–4] has been extensively used to study the nature of molecular bonding, which becomes encoded in angular distributions of the outgoing photofragments. It is one of the most basic chemical processes and is highly amenable to quantum state control of the outgoing particles, since the reaction proceeds without a collision. The majority of photodissociation experiments to date have

been carried out in a regime that is well described in the quasiclassical framework [5–8], while recently we studied this reaction in the purely quantum regime to observe matter-wave interference of the photodissociation products [9] and control of the reaction by weak magnetic fields [10]. In this work, we show that the photodissociation energy can be tuned by several orders of magnitude to span the range from the quantum-mechanical to the quasiclassical regime. Experimentally and theoretically we demonstrate how the crossover occurs and what determines its energy scale. We also find that, if the photofragments are identical bosonic or fermionic particles, then the reaction outcome is not always well described in quasiclassical terms even at high energies and the effects of quantum statistics can persist indefinitely. Moreover, we apply the Wenzel–Kramers–Brillouin (WKB) approximation to photodissociation, as well as a related semiclassical approximation, and discuss how accurately they capture the transition from ultracold to quasiclassical behavior.

In the experiment, we trap diatomic strontium molecules ($^{88}\text{Sr}_2$) at a temperature of a few microkelvin, enabling precise manipulation and preparation of specific quantum states as the starting point for photodissociation. The photodissociation laser light has strictly controlled frequency and polarization, yielding photofragments in fully defined quantum states. The *ab initio* theory is aided by a state-of-the-art molecular model [11,12] that captures the effects of nonadiabatic mixing and yields excellent agreement with spectroscopic measurements [13–16].

This approach offers a unique possibility to finely scan a large range of energies that is relevant to the crossover from

*Present address: Department of Physics, University of Chicago, 929 East 57th Street GCIS ESB11, Chicago, Illinois 60637, USA.

†Present address: Facebook, Inc., 1 Hacker Way, Menlo Park, California 94025, USA.

‡tanya.zelevinsky@columbia.edu

distinctly quantum-mechanical to quasiclassical photodissociation. Since the initial molecular states have low angular momenta, the relevant dynamics occurs at very low, millikelvin energies. The experiment can sample energies from ~ 0.1 mK limited by the molecule trap depth to ~ 100 mK limited by the available laser intensity that is needed to overcome the diminishing photodissociation transition strengths. The rotational and electronic potential barriers that are explored in this work and in the companion paper [17] fall within this range, permitting direct observations of the crossover. We reduce the process to a single initial molecular state and two angular-momentum product channels, in which case the quantum mechanics of the reaction can be encoded in a single pair of coefficients: the amplitude and phase of the channel interference.

Note that in both quantum and quasiclassical regimes we work with single initial quantum states. The classical nature of the process emerges not because of statistical averages over the initial states, but when the kinetic energies of the photofragments are large. At high energies, the photodissociation timescale is much faster than the timescale of molecular rotations, and the molecules can be described as classical rotors. An equivalent view is that the photodissociation outcome should have quasiclassical behavior if the photofragment energy in the continuum exceeds the height of any potential barriers. This regime is referred to as axial recoil, where the molecule has insufficient time to rotate during photodissociation and the photofragments emerge along the instantaneous direction of the bond axis. Here we investigate at what energies the axial-recoil regime is reached, whether it is accurately described by the quasiclassical model, and how its onset depends on the molecular binding energy and angular momentum.

In Sec. II of this work, we describe the photodissociation experiment and show the measured and calculated photofragment angular distributions. In Sec. III, we discuss the quantum-mechanical photodissociation cross section used in calculating the angular distributions, its axial-recoil limit, and the quasiclassical model. Section IV details the crossover from the ultracold to the quasiclassical regime for a range of molecular binding energies and angular momenta and shows the onset of the axial-recoil limit at energies that exceed the potential barriers in the continuum. In Sec. V we discuss the breakdown of the quasiclassical picture of photodissociation in case of identical photofragments and present the correct high-energy limit that takes quantum statistics into account. We summarize our conclusions in Sec. VI.

II. THE PHOTODISSOCIATION EXPERIMENT

The starting point for the experiment is creation of ~ 7000 weakly bound ultracold $^{88}\text{Sr}_2$ molecules in the electronic ground state. This is accomplished by laser cooling, trapping, and photoassociating Sr atoms in a far-off-resonant optical lattice [18]. Subsequently, optical selection rules allow specific molecular quantum states to be populated and serve as a starting point for photodissociation.

Figure 1 shows the photodissociation experiment from the point of view of molecular potentials and wave functions. The ground-state *gerade* potential $X0_g^+$ correlates to the ${}^1S + {}^1S$

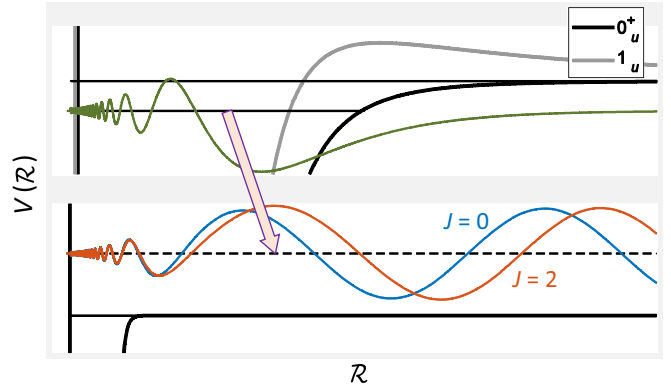


FIG. 1. Molecular potentials for the $^{88}\text{Sr}_2$ electronic states used in this work. The ground state $X0_g^+$ correlates to the ${}^1S + {}^1S$ atomic threshold while the excited states 0_u^+ and 1_u correlate to ${}^1S + {}^3P_1$. The 1_u potential has a ~ 1 mK electronic barrier. The molecules are photodissociated via an electric-dipole optical transition from bound states of mostly 0_u^+ or 1_u character to the ground-state continuum. A range of rovibrational initial states are explored. In this example, weakly bound $0_u^+(v = -2, J_i = 1, M_i = 0)$ molecules are photodissociated, and the photofragments occupy two allowed partial waves $J = \{0, 2\}$ shown at the energy of 50 MHz (2.4 mK).

atomic threshold, while the singly excited *ungerade* potentials 0_u^+ and 1_u correlate to ${}^1S + {}^3P_1$, where the 0 and 1 state labels correspond to Ω , the projection of the total atomic angular momentum onto the molecular axis. Weakly bound ground-state molecules are excited to 0_u^+ and 1_u bound states with a laser pulse, and the resulting molecules are immediately photodissociated to the ground-state continuum. The bound states are labeled by their vibrational quantum number v (negative numbers count down from the threshold), total angular momentum J , and its projection M onto the quantization axis that is set by a small vertical magnetic field. In Fig. 1, the $0_u^+(v = -2, J_i = 1, M_i = 0)$ molecules are photodissociated by 689 nm light. Here the allowed angular-momentum states, or partial waves, in the continuum are $J = \{0, 2\}$ due to electric-dipole selection rules as well as the bosonic nature of ^{88}Sr that allows only even J values in the ground state of the homonuclear dimer.

The photodissociation laser light copropagates with the lattice light and both are focused to a $30 \mu\text{m}$ waist at the molecular cloud. A broad imaging beam, resonant with the strong 461 nm transition in atomic Sr, nearly copropagates with the lattice and is directed at a charge-coupled device camera that collects absorption images of the photofragments. A typical experiment uses $\sim 10 \mu\text{s}$ long photodissociation laser pulses, $\sim 100 \mu\text{s}$ of free expansion, and $\sim 10 \mu\text{s}$ absorption imaging pulses [17]. Several hundred images are averaged in each experiment.

The experimental and theoretical results of photodissociating the molecules in a range of precisely prepared quantum states are shown in Fig. 2. In this set of measurements, light polarization is along the quantization axis and the molecules start from $J_i = 1, M_i = 0$. In Fig. 2(a), molecules in vibrational states $v = \{-2, -3, -4, -5\}$ of 0_u^+ are photodissociated. The photofragment angular distributions show a strong energy dependence, and a less pronounced dependence on

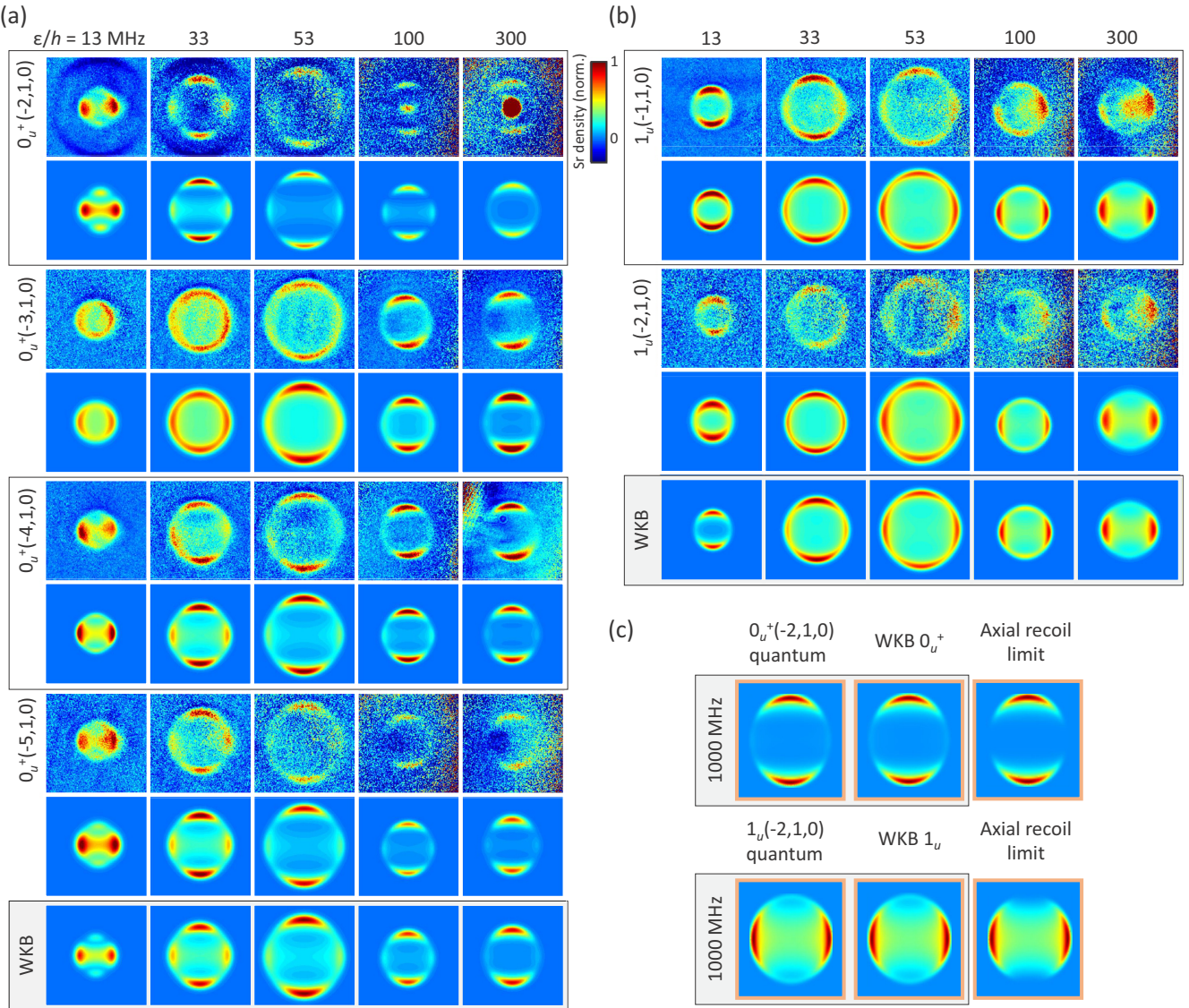


FIG. 2. Measured and calculated photofragment angular distributions in the ultracold quantum-mechanical regime and in the high-energy axial-recoil limit. (a) The 0_u^+ initial states are explored at the continuum energies $\varepsilon/h = \{13, 33, 53, 100, 300\}$ MHz ($\varepsilon/k_B = 0.6\text{--}14$ mK). For each initial state, the upper and lower rows correspond to measurements and quantum-mechanical theory, respectively. The *ab initio* images were adjusted for the shell size and thickness in experimental data, where the photofragment ring diameter is typically 0.3–0.5 mm. The strong dependence of the patterns on ε and the less pronounced dependence on v are discussed in the text. The bottom row shows v -independent distributions obtained with the WKB approximation. The most weakly bound state exhibits a central dot that arises from spontaneous photodissociation into the optical lattice; these are more apparent at higher energies where the signal is weaker and can be ignored. (b) Same as in panel (a), for 1_u initial molecular states. (c) Angular distributions calculated for a pair of 0_u^+ and 1_u weakly bound states using both quantum theory and the WKB approximation at a high energy $\varepsilon/h = 1000$ MHz ($\varepsilon/k_B = 48$ mK), to show their close agreement with the appropriate axial-recoil limit.

v except for the most weakly bound levels, as discussed in Sec. IV A. The bottom row of images is calculated with the WKB approximation, which is independent of v and described in Sec. IV B. Figure 2(b) is analogous to Fig. 2(a) but illustrates the 1_u initial states. A good agreement between measurements and quantum-mechanical calculations is reached for all initial states and continuum energies. Figure 2(c) shows agreement between quantum theory and the WKB approximation at the continuum energy $\varepsilon/h = 1000$ MHz ($\varepsilon/k_B = 48$ mK) where $h = 2\pi\hbar$ and k_B are the Planck and Boltzmann

constants. At this high energy, both methods approach the axial-recoil limit which is also shown.

III. PHOTOFRAGMENT ANGULAR DISTRIBUTIONS

Sections III A–III E overview the quantum-mechanical calculation and parametrization of the photodissociation cross section both in the low-energy regime and in the high-energy axial-recoil limit, as well as the correspondence of the latter to the quasiclassical approximation.

A. General quantum-mechanical model

The general quantum-mechanical expression for the photodissociation cross section is based on Fermi's golden rule with the electric-dipole ($E1$) transition operator,

$$\sigma_{QM}(\theta, \phi) \propto \left| \langle \Psi_k^{JM}(\{\mathbf{r}\}, \mathcal{R}) | \hat{T}_{E1}^1 | \Psi_{J_i M_i \Omega_i}(\{\mathbf{r}\}, \mathcal{R}) \rangle \right|^2, \quad (1)$$

where $\{\mathbf{r}\}$ is the set of atomic electronic coordinates, \mathcal{R} is the vector connecting the photofragments, \mathbf{k} is the laboratory-frame wave vector of the photofragments, Ψ_k^{JM} is the final (continuum) wave function, and $\Psi_{J_i M_i \Omega_i}$ is the initial (bound) wave function. The polar and azimuthal angles $\{\theta, \phi\}$ are referenced to the quantization axis.

Assuming a pure initial state $|J_i M_i \Omega_i\rangle$, expanding the bound and continuum wave functions into the products of their electronic, rovibrational, and angular parts, integrating over the rotation angles and summing over M transforms Eq. (1) into

$$\begin{aligned} \sigma_{QM}(\theta, \phi) &\propto \sum_{\Omega_k} \left| \sum_{J_k(M_k)PQn_k} (-1)^{M_k+\Omega_k} (2J_k+1) D_{M_k \Omega_k}^{J_k}(\phi, \theta, 0) \right. \\ &\quad \times \begin{pmatrix} J_k & 1 & J_i \\ -M_k & P & M_i \end{pmatrix} \begin{pmatrix} J_k & 1 & J_i \\ -\Omega_k & Q & \Omega_i \end{pmatrix} \\ &\quad \times \left. \langle \chi_{n_k \Omega_k}^{J_k}(\mathcal{R}) | \mathbf{d}_{BF} | \chi_{n_i J_i \Omega_i}(\mathcal{R}) \rangle \right|^2, \end{aligned} \quad (2)$$

where $\chi_n(\mathcal{R})$ are the rovibrational wave functions indexed by all the relativistic electronic channels that are included in the model, \mathbf{d}_{BF} is the body-fixed $E1$ transition operator, J_k are the indexed continuum angular momenta (also referred to simply as partial waves J), $D_{M\Omega}^J$ are Wigner rotation matrices, and $Q = \Omega_k - \Omega_i$ (a photodissociation transition is called parallel if $Q = 0$ and perpendicular if $|Q| = 1$). The polarization index $P = 0$ or $P = \pm 1$ if the photodissociation light is polarized along or perpendicularly to the quantization axis, respectively (such that $P = M_k - M_i$).

$$\begin{aligned} R = &\left| \sqrt{2J_i - 1} \begin{pmatrix} J_i - 1 & 1 & J_i \\ -M_k & P & M_i \end{pmatrix} \begin{pmatrix} J_i - 1 & 1 \\ 0 & -\Omega_i \end{pmatrix} \right. \\ &\times \left. \sum_{J_k=\{J_i-1, J_i+1\}} \left| \sqrt{2J_k + 1} \begin{pmatrix} J_k & 1 & J_i \\ -M_k & P & M_i \end{pmatrix} \begin{pmatrix} J_k & 1 & J_i \\ -\Omega_k & Q & \Omega_i \end{pmatrix} \right. \right|^2 \end{aligned}$$

The δ parameter is calculated as the phase shift difference for the continuum wave functions, $\delta = \delta_{J_i+1} - \delta_{J_i-1}$.

In the axial-recoil limit, Eq. (5) is simplified by setting the matrix elements to a constant and canceling them, as explained in Sec. III B. This results in values of R that approach 0.5 with increasing J_i , while the phase shifts become identical: $\delta_{J_i+1} \rightarrow \delta_{J_i-1}$, yielding $\delta \rightarrow 0$ and $\cos \delta \rightarrow 1$.

B. Axial-recoil approximation

At low photofragment energies, to obtain the correct photodissociation cross sections, it is crucial to calculate the matrix elements $\langle \chi_{n_k \Omega_k}^{J_k}(\mathcal{R}) | \mathbf{d}_{BF} | \chi_{n_i J_i \Omega_i}(\mathcal{R}) \rangle$ in Eq. (2). At high energies, these matrix elements become independent of J_k [7] and can be simply factored out. This is equivalent to disregarding the photodissociation dynamics. Under this axial-recoil approximation, the photodissociation cross section (2) reduces to

$$\begin{aligned} \sigma(\theta, \phi)_{AR} \propto &\sum_Q \left| \sum_{J_k P} (-1)^{M_k+\Omega_k} (2J_k+1) D_{M_k \Omega_k}^{J_k}(\phi, \theta, 0) \right. \\ &\times \left. \begin{pmatrix} J_k & 1 & J_i \\ -M_k & P & M_i \end{pmatrix} \begin{pmatrix} J_k & 1 & J_i \\ -\Omega_k & Q & \Omega_i \end{pmatrix} \right|^2. \end{aligned} \quad (3)$$

C. Two-parameter quantum-mechanical model

Consider the photodissociation of $0_u^+(v, J_i, M_i)$ molecules to the ground-state continuum with $P = 0$. For odd J_i (which are the only allowed angular momenta in 0_u^+ due to quantum statistics), the allowed angular momenta of the photofragments are $J = J_i - 1$ and $J_i + 1$, while $M = M_i$. Then the quantum-mechanical photofragmentation cross section can be expressed by using only two parameters, the channel amplitude squared R and the relative channel phase δ :

$$\begin{aligned} \sigma_{R\delta}(\theta, \phi) \propto &\left| \sqrt{R} Y_{J_i-1, M_i}(\theta, \phi) \right. \\ &\left. + (-1)^{\Omega_i} e^{i\delta} \sqrt{1-R} Y_{J_i+1, M_i}(\theta, \phi) \right|^2. \end{aligned} \quad (4)$$

The $(-1)^{\Omega_i}$ factor correctly connects the sign of the δ parameter to the phase shift between the continuum wave functions, and Y_{JM} are spherical harmonics which are proportional to the angular wave functions for $\Omega = 0$.

The expression for the R parameter can be derived by comparing Eq. (4) to the traditional cross section (2). We obtain

$$R = \left| \sum_{J_k=\{J_i-1, J_i+1\}} \left| \sqrt{2J_k + 1} \begin{pmatrix} J_k & 1 & J_i \\ -M_k & P & M_i \end{pmatrix} \begin{pmatrix} J_k & 1 & J_i \\ -\Omega_k & Q & \Omega_i \end{pmatrix} \right. \right|^2 \quad (5)$$

D. Quasiclassical model

The commonly used quasiclassical model for photofragment angular distributions [5,6] describes the photodissociation cross section as

$$\sigma_{QC}(\theta, \phi) \propto P_i(\theta, \phi) [1 + \beta_2 P_2(\cos \theta)], \quad (6)$$

where $P_i(\theta, \phi) = |D_{M_i \Omega_i}^{J_i}(\phi, \theta, 0)|^2$ is the probability density of the initial molecular orientation. The anisotropy parameter is $\beta_2 = 2$ for parallel photodissociation transitions ($Q = 0$)

and $\beta_2 = -1$ for perpendicular transitions ($|Q| = 1$). If the molecule is in a superposition of $|J_i M_i \Omega_i\rangle$ states, the initial probability density can be generalized as [8]

$$P_i(\theta, \phi) = \sum_{J_i J'_i M_i M'_i \Omega_i} D_{M_i \Omega_i}^{J_i}(\phi, \theta, 0) D_{M'_i \Omega_i}^{J'_i *}(\phi, \theta, 0). \quad (7)$$

Note that, in Eq. (7), there are no cross terms for Ω_i . The intuition behind Eq. (6) is that the photofragment angular distribution follows the initial angular density of the molecule, modified by the angular probability density of the photon absorption.

E. Correspondence of quasiclassical model to axial-recoil approximation

It was shown in Ref. [7] that, for photodissociation light polarized along the quantization axis, Eq. (3) reduces to $\sigma_{\text{AR}}(\theta, \phi) \propto |D_{M_i \Omega_i}^{J_i}|^2[1 + \beta_2 P_2(\cos \theta)]$ for initial states with a single Ω_i [8]. We have confirmed that this result also holds for other polarizations of the photodissociating light [if the light polarization is perpendicular to the quantization axis, $P_2(\cos \theta)$ should be replaced with $P_2(\sin \theta \sin \phi)$].

Therefore, the quasiclassical model (6) can be applied in the axial-recoil limit to obtain angular-distribution predictions that are identical to those of the quantum-mechanical model. However, an important assumption in Refs. [7,8] is that the photofragments are not identical quantum particles. Deviations from this assumption are discussed in Sec. V.

IV. CROSSOVER FROM ULTRACOLD REGIME TO AXIAL-RECOIL LIMIT

We investigate the crossover from the ultracold quantum-mechanical to the high-energy axial-recoil regime of photodissociation, as observed in Fig. 2. The intuitive parametrization of Eq. (4) that accurately illustrates two-channel photodissociation allows us to study the crossover as it applies to only two parameters, R and δ . These parameters can have a strong energy dependence in the ultracold regime while approaching their axial-recoil values at higher energies. In this section, we address the following questions: At what energy scale does the outcome of photodissociation approach the axial-recoil limit? How does this energy scale depend on the molecular binding energy (or vibrational level) and rotational angular momentum? How well do the WKB and semiclassical approximations model this crossover?

A. Approaching the axial-recoil limit: Channel amplitude

The R parameter from Eq. (4) depends on both the bound and continuum wave functions, as can be explicitly seen from Eq. (5). Therefore, its behavior as a function of continuum energy can depend on the vibrational state of the molecule, potentially influencing the energy scale at which the axial-recoil limit is reached based on the molecular binding energy. The plots in Fig. 3(a) show the R parameter for several weakly bound initial states $0_u^+(v, J_i = 1, M_i = 0)$ with $v = \{-2, -3, -4, -5\}$ as well as for the most deeply bound state $v = 0$. The dashed line indicates the axial-recoil limit.

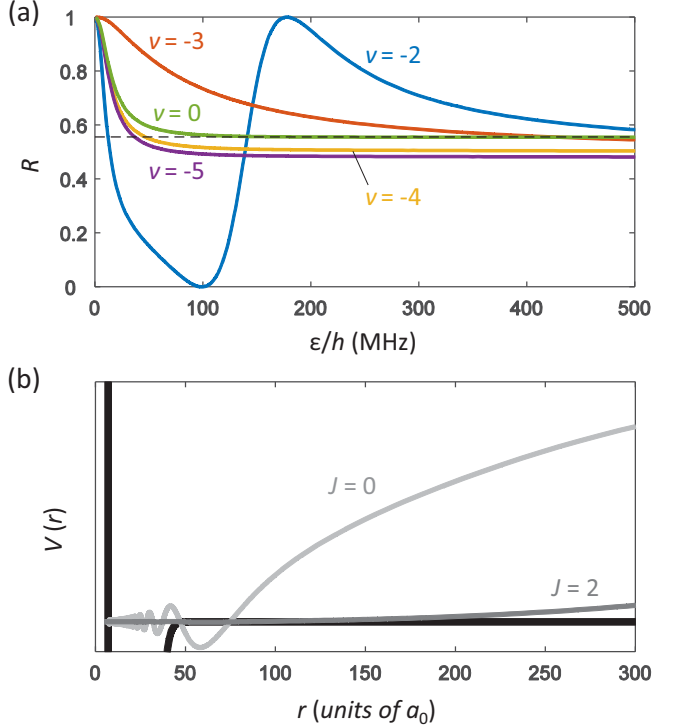


FIG. 3. (a) Quantum-mechanical calculation of the amplitude-squared R parameter for two-channel photodissociation as in Eq. (4). The initial molecular state is $0_u^+(v, 1, 0)$ with $v = \{-2, -3, -4, -5\}$, and $P = 0$. For comparison, the most deeply bound $v = 0$ state is also shown. The axial-recoil limit is indicated with a dashed line. (b) The allowed continuum wave functions with $J = \{0, 2\}$ are plotted for very low energy $\varepsilon/h = 0.5$ MHz ($\varepsilon/k_B = 24$ μ K). The negligible contribution of the $J = 2$ partial wave due to its repulsive rotational barrier explains why $R = 1$ as $\varepsilon \rightarrow 0$ in panel (a) and thus only the lowest allowed partial wave is populated in near-threshold photodissociation.

For some of the shallow vibrational levels such as $v = -2, -3$ (bound by $\sim 10^2$ MHz) the R parameter shows a strong energy dependence that does not closely resemble that of more deeply bound states, as is also observed in Fig. 2. This is caused by the large spatial extent ($\gtrsim 100$ bohr) of weakly bound wave functions, as illustrated for the $0_u^+(-2, 1, 0)$ wave function in Fig. 1. The continuum wave functions, as also shown in Fig. 1, are similar at small internuclear separations but undergo a relative phase shift at larger distances that correspond to the bond length in initially very weakly bound molecules. This can prevent photodissociation from reaching quasiclassical behavior at the expected energies. The energy dependencies for $v = -4, -5$ (bound by $\sim 10^3$ MHz) are more regular, and we find that all the deeper vibrational levels starting from $v = -10$ (bound by $\sim 10^5$ MHz) exhibit nearly identical behavior illustrated in Fig. 3(a) by the deepest $v = 0$ level (bound by $\sim 10^8$ MHz). We conclude that, with the exception of asymptotic molecules that are bound just below threshold, the R parameter is independent of the vibrational quantum number. Since the δ parameter is v independent as discussed in Sec. IV B, the expected anisotropy patterns are nearly independent of v or the binding energy. We have checked that, for higher initial angular momenta J_i , the R

parameter is also independent of v except for the most weakly bound molecules.

It is clear from Fig. 3(a) that $R \rightarrow 1$ as $\varepsilon \rightarrow 0$, indicating that the lowest partial wave ($J = 0$ in this case) dominates the photofragment distribution at ultralow energies. This is caused by the suppression of low-energy continuum wave functions with higher angular momenta at relevant internuclear separations due to their rotational barriers. Figure 3(b) shows the $J = 0$ and $J = 2$ wave functions at a low energy of $\varepsilon/h = 0.5$ MHz ($\varepsilon/k_B = 24 \mu\text{K}$), where $J = 2$ is strongly suppressed at the relevant molecular bond lengths of $\lesssim 100$ bohr.

The crossover from the ultracold, quantum-mechanical regime to the axial-recoil limit is explored in Fig. 4 as a function of the initial angular momentum J_i . The R parameter is plotted as a function of energy for different odd J_i of initial states within the $\{0_u^+, 1_u\}$ electronic manifold, assuming $M_i = P = 0$. The calculations were performed for the most deeply bound vibrational level $v = 0$ to avoid any dependence on v . For all initial states, $R = 1$ at threshold and decays to the axial-recoil limit (shown with horizontal lines) as a function of energy. In each frame, a vertical line marks the rotational barrier height corresponding to the largest partial wave in the continuum, $J_i + 1$. As expected, the barrier height sets the energy scale for the onset of the axial-recoil regime. This trend is evident despite the irregularities connected to shape resonances for $J = \{4, 8, 20\}$ (the $J = 4$ shape resonance has been experimentally confirmed [9]).

B. Approaching the axial-recoil limit: Channel phase and various approximations

The δ parameter in Eq. (4) is the phase difference between the continuum channel wave functions and is independent of the initial state of the photodissociated molecules. It is thus readily amenable to a range of approximation techniques. We consider the WKB approximation [19,20] and the semiclassical approximation [21] and investigate their applicability to photodissociation across a wide span of energies as well as their convergence to the axial-recoil limit.

The WKB approximation is a method of solving linear differential equations with spatially varying coefficients. It is applicable to approximating the solutions to the time-independent Schrödinger equation, where the wave function is represented as an exponential with smoothly varying amplitude and phase, and is a particularly useful method of finding δ without using the full quantum-mechanical treatment.

The continuum wave function corresponding to the partial wave J has the asymptotic behavior

$$\psi_J(\mathcal{R}) \propto \sin\left(k\mathcal{R} + \delta_J - \frac{J\pi}{2}\right), \quad (8)$$

where $k \equiv \sqrt{2\mu\varepsilon}/\hbar$ and μ is the reduced mass. An analytical expression for δ_J is based on the WKB approximation where the wave function is assumed to have the form $\psi_J(\mathcal{R}) = e^{iS(\mathcal{R})/\hbar}$. If only the lowest-order term in \hbar is kept in $S(\mathcal{R})$, then $\psi(\mathcal{R}) \propto \sin[\int_{\mathcal{R}_0}^{\mathcal{R}} p(\mathcal{R})d\mathcal{R}/\hbar + \pi/4]$ where \mathcal{R}_0 is the classical turning point and $p(\mathcal{R}) \equiv \{2\mu[E - V(\mathcal{R})] - J(J+1)/\mathcal{R}^2\}^{1/2}$ in terms of the molecular potential $V(\mathcal{R})$. The WKB approximation is most applicable at higher energies and breaks down near the turning point

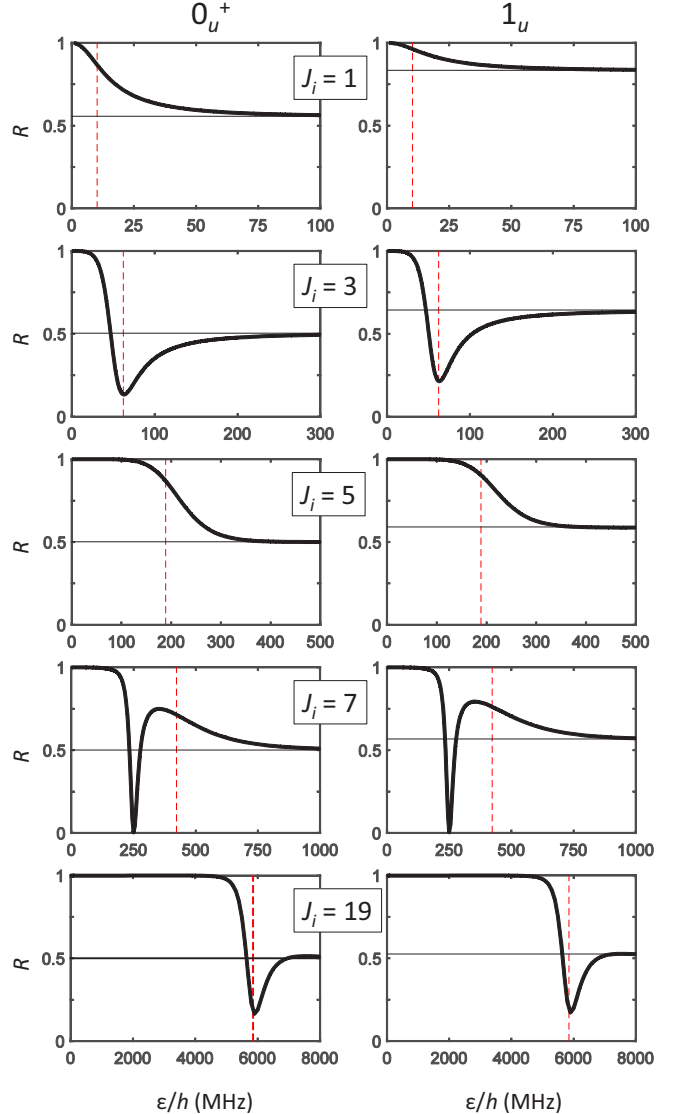


FIG. 4. Dependence of the amplitude-squared R parameter from Eq. (4) on energy and on initial angular momentum J_i . The initial molecular states are $0_u^+(0, J_i, 0)$ (left column) and $1_u(0, J_i, 0)$ (right column), and $P = 0$. In each frame, the axial-recoil limit is indicated by a horizontal line, and the highest rotational barrier in the continuum is shown by a dashed vertical line. For larger J_i , the axial-recoil limit is approached at higher energies, but in all cases the crossover from the ultracold to the quasiclassical regime occurs at the energy scale set by the barrier height. The initial states with $J_i = 3, 7, 19$ exhibit shape-resonance behavior.

where $p(\mathcal{R}) \approx 0$. Based on the WKB expression for $\psi(\mathcal{R})$ and Eq. (8), the asymptotic phase shift is

$$\delta_J^{\text{WKB}} = \lim_{\mathcal{R} \rightarrow \infty} \left[\frac{1}{\hbar} \int_{\mathcal{R}_0}^{\mathcal{R}} p(\mathcal{R})d\mathcal{R} + \frac{\pi}{4} - k\mathcal{R} + \frac{J\pi}{2} \right]. \quad (9)$$

A related approach to investigating the quantum-quasiclassical crossover is to consider the classical rotation of the molecule during photodissociation. We refer to this method as the semiclassical approximation. Its value is in the intuitive interpretation of the molecular rotation angle during the bond-breaking process and a slightly faster computational

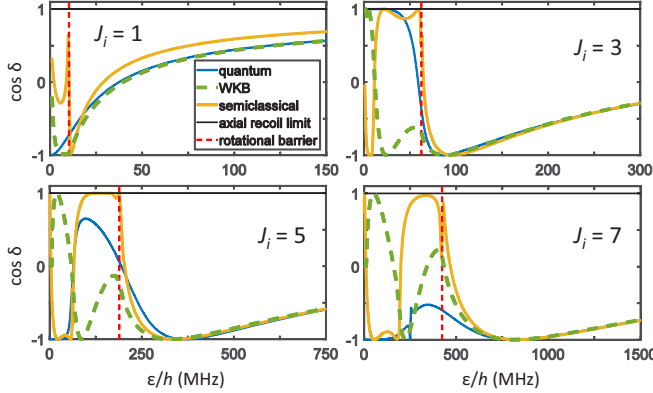


FIG. 5. A comparison of the quantum-mechanical, WKB, and semiclassical methods for evaluating $\cos \delta$ for a range of initial molecular angular momenta J_i within the 0_u^+ electronic manifold (here $M_i = P = 0$). The phase angle δ quantifies interference between the two allowed dissociation channels and plays a key role in the observed photofragment angular distributions. Both approximations approach the quantum-mechanical result at increasingly higher energies that are set by the rotational barrier heights (dashed vertical lines). All methods recover the axial-recoil limit (horizontal lines) at high energies, but this convergence is slower for the δ parameter than for the R parameter in Fig. 4.

convergence than the WKB method. The angle of rotation γ between the initial molecular axis and the axis created by the scattered fragments is $\gamma_J = \int_{\mathcal{R}_0}^{\infty} \hbar \sqrt{J(J+1)} / [p(\mathcal{R})\mathcal{R}^2] d\mathcal{R}$. This angle is connected to the anisotropy parameter β_2 by the relation $\beta_2 = \beta_{\text{AR}} P_2(\cos \gamma)$, where β_{AR} takes on the limiting values from the quasiclassical model [4–6] such that $\beta_{\text{AR}} = \{2, -1\}$ for parallel and perpendicular photodissociation transitions, respectively. This semiclassical approximation is more general than the quasiclassical model which assumes that $\gamma = 0$.

The WKB method links the classical parameter γ to the quantum-mechanical phase δ_J through $\gamma = -d\delta_J/dJ$ [20]. Further approximating the derivative by a difference quotient yields the semiclassical approximation for the phase shifts,

$$\delta_J - \delta_{J'} = (J' - J) \frac{\gamma_J + \gamma_{J'}}{2}. \quad (10)$$

The semiclassical approximation has been successfully applied to diatomic molecule photodissociation at the energy of several wave numbers above threshold [21], where a deviation from the axial-recoil limit was observed, yielding an agreement with quantum-mechanical calculations [22]. To summarize, the hierarchy of approximations, from the most to the least exact, is (i) the quantum-mechanical treatment, (ii) the WKB approximation, (iii) the semiclassical model, and (iv) the axial-recoil approximation (which is generally equivalent to the quasiclassical model with exceptions discussed in Sec. V and Ref. [8]).

Figure 5 compares the quantum-mechanical [Eq. (4)], WKB [Eq. (9)], and semiclassical [Eq. (10)] approaches to calculating the δ parameter. This phase angle is determined for initial molecular states $J_i = \{1, 3, 5, 7\}$ within the 0_u^+ electronic manifold, assuming photodissociation with $M_i = P = 0$. We find the applicability ranges of both approximation

methods to be similar, with the exception that the WKB approximation is more accurate for very low J_i . These ranges are set by the barrier heights in the continuum, indicated with dashed vertical lines. We also find that all methods converge to the axial-recoil limit $\cos \delta = 1$. However, this convergence happens more slowly than for the R parameter in Fig. 4 and dominates the discrepancy between the measured angular distributions and those expected for axial recoil at energies beyond the barrier height, as in Fig. 2 where the barrier height is only ~ 10 MHz but nonclassical behavior persists to $\sim 10^3$ MHz [23]. Furthermore, only the quantum-mechanical approach is sensitive to shape resonances; for example, one that is visible in Fig. 5 at $\varepsilon/h \approx 250$ MHz for $J_i = 7$.

V. THE ROLE OF QUANTUM STATISTICS IN PHOTODISSOCIATION

The equivalence of the quasiclassical approximation to the axial-recoil limit of the quantum-mechanical model holds for molecules in well-defined Ω_i states under the assumption that the photofragments are not identical bosons or fermions. Section III E assumes that a molecule with angular momentum $J_i \neq 0$ can dissociate into the $\{J_i - 1, J_i, J_i + 1\}$ partial waves as allowed by $E1$ selection rules.

Spin statistics can impose additional limitations on the available continuum channels, as is the case for Sr_2 and many other molecules. In the electronic ground state, J is always even for Sr_2 composed of identical bosonic Sr atoms and odd for Sr_2 composed of identical fermions, while in the 0_u^+ excited state only odd J exist for the bosons and even J for the fermions. In this work, we use bosonic ^{88}Sr and therefore ground-state J are even. Furthermore, in cases where $\Omega_i = \Omega_k = 0$ or $M_i = M_k = P = 0$, the properties of the $3j$ symbols in Eqs. (2) and (3) [24] naturally force the J of the photofragments to be only even or only odd, making the axial-recoil approximation insensitive to quantum statistics [25]. Here we apply Eq. (3) to cases where quantum statistics must be considered, and compare the results to the quasiclassical model (6). In our experiment, this affects photodissociation from the 1_u electronic state to the ground-state continuum, except in cases where $M_i = P = 0$.

First we assume that the photodissociation light polarization points along the quantization axis. The two relevant cases are $J = J_i$ (applicable, for example, to fermionic-Sr dimers dissociating from odd J_i) and $J = \{J_i - 1, J_i + 1\}$ (applicable to bosonic-Sr dimers photodissociating from odd J_i as in our experiments). As shown in the Appendix, we apply the axial-recoil cross section $\sigma_{\text{AR}}(\theta, \phi)$ to both cases that are governed by quantum statistics via restricting the sum over J_k in Eq. (3) and find the modified photodissociation cross section $\sigma_{\text{QS},\parallel}(\theta, \phi)$. The result can be written in a form that resembles the quasiclassical cross section $\sigma_{\text{QC}}(\theta, \phi)$ in Eq. (6) but with the initial angular probability density $P_i(\theta, \phi) = |D_{M_i, \Omega_i}^{J_i}(\phi, \theta, 0)|^2$ replaced by

$$P'_{i,\parallel}(\theta, \phi) = \left| D_{M_i, 1}^{J_i}(\phi, \theta, 0) - \sigma_i D_{M_i, -1}^{J_i}(\phi, \theta, 0) \right|^2, \quad (11)$$

where $\sigma_i \equiv p_i (-1)^{J_i}$ is the spectroscopic parity of the initial state and p_i is the parity with respect to space-fixed inversion.

For example, for 1_u initial states, $p_i = -1$ for bosonic-Sr dimers and $p_i = 1$ for fermionic-Sr dimers.

Next we treat the case where the photodissociation light polarization is perpendicular to the quantization axis. Again spin statistics enforces either $J = J_i$ or $J = \{J_i - 1, J_i + 1\}$. As detailed in the Appendix, we adapt $\sigma_{\text{AR}}(\theta, \phi)$ to both cases and find the modified photodissociation cross section

$$\begin{aligned} \sigma_{\text{QS},\perp}(\theta, \phi) &\propto \cos^2 \phi \left| D_{M_i,1}^{J_i}(\phi, \theta, 0) + \sigma_i D_{M_i,-1}^{J_i}(\phi, \theta, 0) \right|^2 \\ &+ \cos^2 \theta \sin^2 \phi \left| D_{M_i,1}^{J_i}(\phi, \theta, 0) - \sigma_i D_{M_i,-1}^{J_i}(\phi, \theta, 0) \right|^2. \end{aligned} \quad (12)$$

This result does not directly resemble the quasiclassical cross section $\sigma_{\text{QC}}(\theta, \phi)$. However, as expected, Eq. (6) is recovered for either light polarization when the appropriate quantum-statistics-adapted cross section is summed over the initial state parity p_i .

The photodissociation cross sections modified by spin statistics are thus not correctly described by the quasiclassical model (6), even in the axial-recoil limit of large continuum energies. This effect is observable in experiments as a deviation of high-energy photodissociation images from the quasiclassical picture for certain initial molecular states and light polarizations [17].

Figure 6 illustrates $^{88}\text{Sr}_2$ photodissociation pathways where photofragment angular distributions in the axial-recoil limit cannot be described by the quasiclassical model (6) but are accurately reflected in the quantum-mechanical model [Eqs. (3), (11), and (12)]. In our experiment and in the figure, the initial molecular states and laser polarizations that lead to a nonquasiclassical axial-recoil limit are (a) $1_u(J_i = 1, M_i = \{0, 1\}, P = 1)$, (b) $1_u(J_i = 3, M_i = \{1, 2\}, P = 0)$, and (c) $1_u(J_i = 3, M_i = \{0, 1, 2, 3\}, P = 1)$. The case considered in the top row of Fig. 6(a) results in a distribution that does not evolve with energy, since only a single partial wave $J = 2$ is allowed in the continuum by selection rules and hence the matrix elements in Eq. (5) cancel for all energies [26]. Our experimental measurements of angular distributions always agree with quantum-mechanical calculations [17]. For photodissociation of molecules in analogous quantum states but composed of identical fermionic isotopes we expect to observe different distributions than in Fig. 6, and still different results, that are well described by the quasiclassical model, are expected for mixed dimers.

VI. CONCLUSIONS

We report photodissociation of ultracold $^{88}\text{Sr}_2$ molecules in isolated internal quantum states, including different binding energies and angular momenta, where we image and calculate the photofragment angular distributions as a function of the kinetic energy in the continuum, spanning from the ultracold to the quasiclassical regime. At the higher energies that exceed the relevant potential barriers, the distributions converge to angular patterns that correspond to the axial-recoil limit where the molecule has no time to rotate during the bond-breaking process. In contrast, at the lower energies the distributions

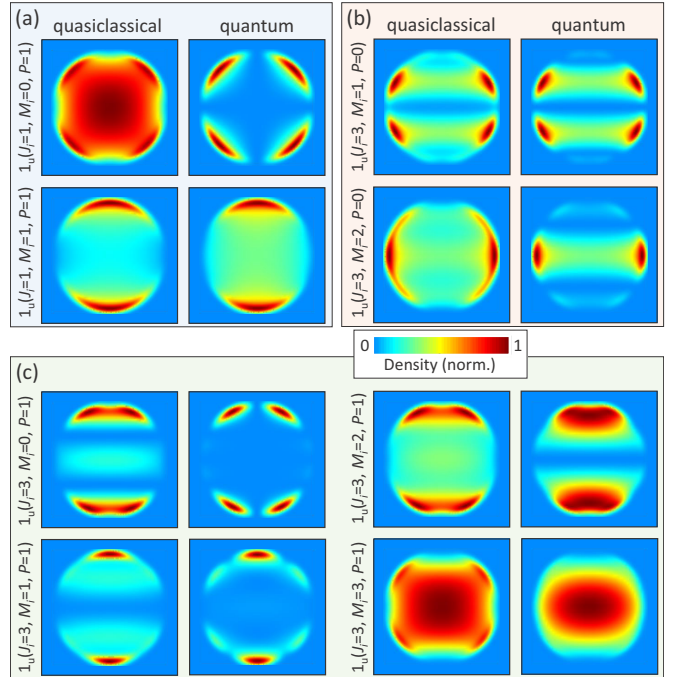


FIG. 6. Quasiclassical and quantum-mechanical calculations of the photofragment angular distributions do not generally converge in the axial-recoil limit if the photofragments are identical particles. Experimental measurements always agree with the quantum theory [17]. Here the high-energy angular distributions are calculated with the quasiclassical [Eq. (6)] and quantum-mechanical [Eqs. (3), (11), and (12)] models for the 1_u initial states with (a) $J_i = 1, M_i = \{0, 1\}, P = 1$, (b) $J_i = 3, M_i = \{1, 2\}, P = 0$, and (c) $J_i = 3, M_i = \{0, 1, 2, 3\}, P = 1$.

exhibit strong variation with energy and a dependence on the initial molecular state.

We utilize precise quantum state selection to ensure a two-channel photodissociation outcome that can be described by only two parameters: an amplitude that has a weak dependence on the initial vibrational quantum number and a phase that only depends on the continuum wave functions. The amplitude converges to the axial-recoil limit significantly faster than the phase, with a slower convergence for very weakly bound initial molecular states. The WKB and semiclassical approximations are shown to agree with the quantum-mechanical model at energies that exceed the barrier heights, and to correctly approach the axial-recoil limit. Finally, we find that in case of identical photofragments, the effects of bosonic or fermionic statistics can persist into the high-energy regime, in which case the axial-recoil limit disagrees with the ubiquitous quasiclassical model.

The ability to observe the crossover from the ultracold to the quasiclassical regime of photodissociation was enabled by quantum state control of the molecules, making it possible to populate exclusively low-angular-momentum states and thus access low partial waves in the continuum that are strongly sensitive to quantum effects. As more experiments begin to probe cold and ultracold chemistry, including molecular photodissociation, it is important to recognize the extent of the parameter space where the processes are truly quantum

mechanical. Our work brings this insight into a long-debated issue of the applicability of quasiclassical models to molecular photodissociation, and elucidates which parameters control the convergence toward the high-energy limit.

ACKNOWLEDGMENTS

We acknowledge the ONR Grant No. N00014-17-1-2246 and the NSF Grant No. PHY-1349725. R.M. and I.M. also acknowledge the Polish National Science Center Grant No. 2016/20/W/ST4/00314 and M.M. the NSF IGERT Grant No. DGE-1069240.

APPENDIX A: AXIAL-RECOIL LIMIT FOR IDENTICAL PHOTOFRAGMENTS

1. Light polarization along the quantization axis

With the assumptions $\{\Omega_i = 1, \Omega_k = 0, M_k = M_i\}$, as for Sr_2 photodissociation from the 1_u states to the ground-state continuum with light polarization along the quantization axis ($P = 0$), the axial-recoil photodissociation cross section (3) becomes

$$\sigma(\theta, \phi) \propto \left| \sum_{J_k} (-1)^{M_i} (2J_k + 1) D_{M_i 0}^{J_k}(\phi, \theta, 0) \times \begin{pmatrix} J_k & 1 & J_i \\ -M_i & 0 & M_i \end{pmatrix} \begin{pmatrix} J_k & 1 & J_i \\ 0 & -1 & 1 \end{pmatrix} \right|^2. \quad (\text{A1})$$

$$\begin{aligned} \sigma(\theta, \phi) &\propto \left| \sum_{J_k=\{J_i-1, J_i, J_i+1\}} (-1)^{M_i} (2J_k + 1) D_{M_i 0}^{J_k}(\phi, \theta, 0) \begin{pmatrix} J_k & 1 & J_i \\ -M_i & 0 & M_i \end{pmatrix} \begin{pmatrix} J_k & 1 & J_i \\ 0 & -1 & 1 \end{pmatrix} \right. \\ &\quad \left. - (-1)^{M_i} (2J_i + 1) D_{M_i 0}^{J_i}(\phi, \theta, 0) \begin{pmatrix} J_i & 1 & J_i \\ -M_i & 0 & M_i \end{pmatrix} \begin{pmatrix} J_i & 1 & J_i \\ 0 & -1 & 1 \end{pmatrix} \right|^2 \\ &= \left| D_{0, -1}^1(\phi, \theta, 0) D_{M_i, 1}^{J_i}(\phi, \theta, 0) + (-1)^{M_i} (2J_i + 1) [D_{M_i, -1}^{J_i}(\phi, \theta, 0) + D_{M_i, 1}^{J_i}(\phi, \theta, 0)] \sin \theta \right. \\ &\quad \left. \times \frac{\sqrt{J_i(J_i + 1)}}{2M_i} \begin{pmatrix} J_i & 1 & J_i \\ -M_i & 0 & M_i \end{pmatrix} \begin{pmatrix} J_i & 1 & J_i \\ 0 & -1 & 1 \end{pmatrix} \right|^2 \\ &= \left| -\frac{1}{\sqrt{2}} \sin \theta D_{M_i, 1}^{J_i}(\phi, \theta, 0) + \frac{1}{2\sqrt{2}} \sin \theta [D_{M_i, -1}^{J_i}(\phi, \theta, 0) + D_{M_i, 1}^{J_i}(\phi, \theta, 0)] \right|^2 \\ &= \frac{1}{8} \left| D_{M_i, 1}^{J_i}(\phi, \theta, 0) - D_{M_i, -1}^{J_i}(\phi, \theta, 0) \right|^2 \sin^2 \theta. \end{aligned} \quad (\text{A4})$$

The second step of Eq. (A4) uses Eq. (A2) as well as the summation (Clebsch–Gordan series)

$$\begin{aligned} &\sum_{J_k} (-1)^{M_k + \Omega_k} (2J_k + 1) D_{M_k \Omega_k}^{J_k}(\phi, \theta, 0) \begin{pmatrix} J_k & 1 & J_i \\ -M_k & P & M_i \end{pmatrix} \begin{pmatrix} J_k & 1 & J_i \\ -\Omega_k & Q & \Omega_i \end{pmatrix} \\ &= \sum_{J_k} D_{-M_k - \Omega_k}^{J_k \star}(\phi, \theta, 0) \begin{pmatrix} J_k & 1 & J_i \\ -M_k & P & M_i \end{pmatrix} \begin{pmatrix} J_k & 1 & J_i \\ -\Omega_k & Q & \Omega_i \end{pmatrix} \\ &= D_{M_i \Omega_i}^{J_i} D_P^1 Q. \end{aligned} \quad (\text{A5})$$

The cross section in Eq. (A4) also has the general form of Eq. (6) with $\beta_2 = -1$ and the initial angular probability density replaced by Eq. (11).

a. Partial waves restricted to J_i

After restricting the allowed partial waves to $J_k = J_i$ and transforming the D matrix as

$$\begin{aligned} D_{M_i 0}^{J_i}(\phi, \theta, 0) &= -\frac{\sqrt{J_i(J_i + 1)}}{2M_i} \sin \theta \\ &\times \left[D_{M_i, -1}^{J_i}(\phi, \theta, 0) + D_{M_i, 1}^{J_i}(\phi, \theta, 0) \right], \end{aligned} \quad (\text{A2})$$

Eq. (A1) reads

$$\sigma(\theta, \phi) \propto \left| D_{M_i, 1}^{J_i}(\phi, \theta, 0) + D_{M_i, -1}^{J_i}(\phi, \theta, 0) \right|^2 \sin^2 \theta. \quad (\text{A3})$$

This cross section has the general form of Eq. (6) with $\beta_2 = -1$ (as expected for this $\Delta\Omega = 1$ transition), with the initial angular probability density replaced by the expression in Eq. (11).

b. Partial waves restricted to $J_i \pm 1$

After restricting the partial waves to $J_k = J_i \pm 1$, the cross section in Eq. (A1) can be manipulated by taking the sum over all partial waves and subtracting the forbidden contributions,

2. Light polarization normal to the quantization axis

With the assumptions $\{\Omega_i = 1, \Omega_k = 0, M_k = M_i \pm 1\}$, as for Sr_2 photodissociation from the 1_u states to the ground-state continuum with light polarization normal to the quantization axis ($P = \pm 1$), the axial-recoil cross section (3) becomes

$$\sigma(\theta, \phi) \propto \left| \sum_{J_k P} (-1)^{M_k} (2J_k + 1) D_{M_k 0}^{J_k}(\phi, \theta, 0) \begin{pmatrix} J_k & 1 & J_i \\ -M_k & P & M_i \end{pmatrix} \right|^2. \quad (\text{A6})$$

a. Partial waves restricted to J_i

After restricting the partial waves to $J_k = J_i$, summing over P , and evaluating the $3j$ symbols, the cross section in Eq. (A6) becomes

$$\sigma(\theta, \phi) \propto (2J_i + 1) \begin{pmatrix} J_i & 1 & J_i \\ 0 & -1 & 1 \end{pmatrix} \left| D_{M_i+1,0}^{J_i}(\phi, \theta, 0) \sqrt{(J_i - M_i)(J_i + M_i + 1)} - D_{M_i-1,0}^{J_i}(\phi, \theta, 0) \sqrt{(J_i + M_i)(J_i - M_i + 1)} \right|^2. \quad (\text{A7})$$

We use recursion formulas [27]

$$D_{M_i+1,0}^{J_i}(\phi, \theta, 0) e^{i\phi} = \frac{\sqrt{J_i(J_i + 1)}}{\sqrt{(J_i - M_i)(J_i + M_i + 1)}} \left[\frac{1 + \cos \theta}{2} D_{M_i,-1}^{J_i}(\phi, \theta, 0) - \frac{1 - \cos \theta}{2} D_{M_i,1}^{J_i}(\phi, \theta, 0) \right], \quad (\text{A8})$$

$$D_{M_i-1,0}^{J_i}(\phi, \theta, 0) e^{-i\phi} = \frac{\sqrt{J_i(J_i + 1)}}{\sqrt{(J_i + M_i)(J_i - M_i + 1)}} \left[\frac{1 + \cos \theta}{2} D_{M_i,1}^{J_i}(\phi, \theta, 0) - \frac{1 - \cos \theta}{2} D_{M_i,-1}^{J_i}(\phi, \theta, 0) \right] \quad (\text{A9})$$

to transform Eq. (A7) into

$$\begin{aligned} \sigma(\theta, \phi) &\propto \left| D_{M_i,1}^{J_i}(\phi, \theta, 0) (\cos \phi + i \cos \theta \sin \phi) - D_{M_i,-1}^{J_i}(\phi, \theta, 0) (\cos \phi - i \cos \theta \sin \phi) \right|^2 \\ &\propto \cos^2 \phi \left| D_{M_i,1}^{J_i}(\phi, \theta, 0) - D_{M_i,-1}^{J_i}(\phi, \theta, 0) \right|^2 + \cos^2 \theta \sin^2 \phi \left| D_{M_i,1}^{J_i}(\phi, \theta, 0) + D_{M_i,-1}^{J_i}(\phi, \theta, 0) \right|^2. \end{aligned} \quad (\text{A10})$$

b. Partial waves restricted to $J_i \pm 1$

With the partial waves limited to $J_k = J_i \pm 1$, the cross section in Eq. (A6) can again be manipulated by taking the sum over all partial waves and subtracting the forbidden contributions,

$$\begin{aligned} \sigma(\theta, \phi) &\propto \left| \sum_{J_k P} (-1)^{M_k} (2J_k + 1) D_{M_k 0}^{J_k}(\phi, \theta, 0) \begin{pmatrix} J_k & 1 & J_i \\ -M_k & P & M_i \end{pmatrix} \begin{pmatrix} J_k & 1 & J_i \\ 0 & -1 & 1 \end{pmatrix} \right. \\ &\quad \left. - (-1)^{M_k} (2J_i + 1) D_{M_k 0}^{J_i}(\phi, \theta, 0) \begin{pmatrix} J_i & 1 & J_i \\ -M_k & P & M_i \end{pmatrix} \begin{pmatrix} J_i & 1 & J_i \\ 0 & -1 & 1 \end{pmatrix} \right|^2. \end{aligned} \quad (\text{A11})$$

After applying Eq. (A2) to the first term and Eqs. (A8) and (A9) to the second term on the right-hand side of Eq. (A11), we obtain the cross section

$$\begin{aligned} \sigma(\theta, \phi) &\propto \left| D_{M_i,1}^{J_i}(\phi, \theta, 0) [D_{1,-1}^1(\phi, \theta, 0) + D_{-1,-1}^1(\phi, \theta, 0)] + \frac{1}{2} D_{M_i,1}^{J_i}(\phi, \theta, 0) (\cos \phi + i \cos \theta \sin \phi) \right. \\ &\quad \left. - \frac{1}{2} D_{M_i,-1}^{J_i}(\phi, \theta, 0) (\cos \phi - i \cos \theta \sin \phi) \right|^2 \\ &= \left| D_{M_i,1}^{J_i}(\phi, \theta, 0) (\cos \phi + i \cos \theta \sin \phi) + D_{M_i,-1}^{J_i}(\phi, \theta, 0) (\cos \phi - i \cos \theta \sin \phi) \right|^2 \\ &\propto \cos^2 \phi \left| D_{M_i,1}^{J_i}(\phi, \theta, 0) + D_{M_i,-1}^{J_i}(\phi, \theta, 0) \right|^2 + \cos^2 \theta \sin^2 \phi \left| D_{M_i,1}^{J_i}(\phi, \theta, 0) - D_{M_i,-1}^{J_i}(\phi, \theta, 0) \right|^2. \end{aligned} \quad (\text{A12})$$

- [1] N. Balakrishnan, Perspective: Ultracold molecules and the dawn of cold controlled chemistry, *J. Chem. Phys.* **145**, 150901 (2016).
- [2] H. Sato, Photodissociation of simple molecules in the gas phase, *Chem. Rev. (Washington, DC, US)* **101**, 2687 (2001).

- [3] R. N. Zare and D. R. Herschbach, Doppler line shape of atomic fluorescence excited by molecular photodissociation, *Proc. IEEE* **51**, 173 (1963).
- [4] R. N. Zare, Photoejection dynamics, *Mol. Photochem.* **4**, 1 (1972).

- [5] S. E. Choi and R. B. Bernstein, Theory of oriented symmetric-top molecule beams: Precession, degree of orientation, and photofragmentation of rotationally state-selected molecules, *J. Chem. Phys.* **85**, 150 (1986).
- [6] R. N. Zare, Photofragment angular distributions from oriented symmetric-top precursor molecules, *Chem. Phys. Lett.* **156**, 1 (1989).
- [7] T. Seideman, The analysis of magnetic-state-selected angular distributions: A quantum mechanical form and an asymptotic approximation, *Chem. Phys. Lett.* **253**, 279 (1996).
- [8] J. A. Beswick and R. N. Zare, On the quantum and quasiclassical angular distributions of photofragments, *J. Chem. Phys.* **129**, 164315 (2008).
- [9] M. McDonald, B. H. McGuyer, F. Apfelbeck, C.-H. Lee, I. Majewska, R. Moszynski, and T. Zelevinsky, Photodissociation of ultracold diatomic strontium molecules with quantum state control, *Nature (London)* **534**, 122 (2016).
- [10] M. McDonald, I. Majewska, C.-H. Lee, S. S. Kondov, B. H. McGuyer, R. Moszynski, and T. Zelevinsky, Control of Ultracold Photodissociation with Magnetic Fields, *Phys. Rev. Lett.* **120**, 033201 (2018).
- [11] W. Skomorowski, F. Pawłowski, C. P. Koch, and R. Moszynski, Rovibrational dynamics of the strontium molecule in the $A^1\Sigma_u^+$, $c^3\Pi_u$, and $a^3\Sigma_u^+$ manifold from state-of-the-art *ab initio* calculations, *J. Chem. Phys.* **136**, 194306 (2012).
- [12] M. Borkowski, P. Morzyński, R. Ciuryło, P. S. Julienne, M. Yan, B. J. DeSalvo, and T. C. Killian, Mass scaling and nonadiabatic effects in photoassociation spectroscopy of ultracold strontium atoms, *Phys. Rev. A* **90**, 032713 (2014).
- [13] B. H. McGuyer, C. B. Osborn, M. McDonald, G. Reinaudi, W. Skomorowski, R. Moszynski, and T. Zelevinsky, Nonadiabatic Effects in Ultracold Molecules Via Anomalous Linear and Quadratic Zeeman Shifts, *Phys. Rev. Lett.* **111**, 243003 (2013).
- [14] B. H. McGuyer, M. McDonald, G. Z. Iwata, W. Skomorowski, R. Moszynski, and T. Zelevinsky, Control of Optical Transitions with Magnetic Fields in Weakly Bound Molecules, *Phys. Rev. Lett.* **115**, 053001 (2015).
- [15] B. H. McGuyer, M. McDonald, G. Z. Iwata, M. G. Tarallo, A. T. Grier, F. Apfelbeck, and T. Zelevinsky, High-precision spectroscopy of ultracold molecules in an optical lattice, *New J. Phys.* **17**, 055004 (2015).
- [16] B. H. McGuyer, M. McDonald, G. Z. Iwata, M. G. Tarallo, W. Skomorowski, R. Moszynski, and T. Zelevinsky, Precise study of asymptotic physics with subradiant ultracold molecules, *Nat. Phys.* **11**, 32 (2015).
- [17] S. S. Kondov, C.-H. Lee, M. McDonald, B. H. McGuyer, I. Majewska, R. Moszynski, and T. Zelevinsky, Crossover from the ultracold to the quasiclassical regime in state-selected photodissociation, *Phys. Rev. Lett.* **121**, 143401 (2018).
- [18] G. Reinaudi, C. B. Osborn, M. McDonald, S. Kotochigova, and T. Zelevinsky, Optical Production of Stable Ultracold $^{88}\text{Sr}_2$ Molecules, *Phys. Rev. Lett.* **109**, 115303 (2012).
- [19] M. S. Child, *Molecular Collision Theory* (Dover Publications, Mineola, New York, 2010).
- [20] E. E. Nikitin and S. Y. Umanskii, *Theory of Slow Atomic Collisions* (Springer-Verlag, Berlin Heidelberg, 1984).
- [21] E. Wrede, E. R. Wouters, M. Beckert, R. N. Dixon, and M. N. R. Ashfold, Quasiclassical and quantum mechanical modeling of the breakdown of the axial-recoil approximation observed in the near threshold photolysis of IBr and Br_2 , *J. Chem. Phys.* **116**, 6064 (2002).
- [22] In Ref. [21] the semiclassical model is referred to as “quasiclassical.” However, it is not equivalent to the quasiclassical description from Refs. [5,6] and is a more accurate approximation.
- [23] For the WKB images in Fig. 2, the axial-recoil value of R was used, since R approaches the high-energy limit faster than δ .
- [24] For a $3j$ symbol $((J_1, J_2, J_3); (M_1, M_2, M_3))$, the sum $J_1 + J_2 + J_3$ must be even if $M_1 = M_2 = M_3 = 0$. Together with Eqs. (2) and (3) this implies that for $E1$ transitions with either $M_i = M_k = 0$ or $\Omega_i = \Omega_k = 0$, the $J_k = J_i$ branch is not allowed.
- [25] For $M_i = P = 0$, quantum statistics combined with the $3j$ symbol properties [24] can cause a normally allowed photodissociation pathway to become forbidden, for example for initial states $1_u(v, J_i, 0)$ with even J_i in bosonic-Sr dimers. Such transitions, however, can be enabled with weak magnetic fields [9,10].
- [26] Two other configurations with this property, $1_u(J_i = 1, M_i = 1, P = 0)$ and $1_u(J_i = 3, M_i = 3, P = 0)$, are not shown.
- [27] D. A. Varshalovich, A. N. Moskalev, and V. K. Khersonskii, *Quantum Theory of Angular Momentum* (World Scientific, Singapore, 1988).